# Correlative characterization of plasma etching resistance of various aluminum garnets

Christian Stern<sup>1,2</sup>, Christian Schwab<sup>1</sup>, Moritz Kindelmann<sup>1,3,4</sup>, Mark Stamminger<sup>5,6</sup>, Thomas E. Weirich<sup>4</sup>, Inhee Park<sup>7</sup>, Florian Hausen<sup>7,8</sup>, Martin Finsterbusch<sup>1</sup>, Martin Bram<sup>1</sup>, Olivier Guillon<sup>1,2,9</sup>

- 1 Forschungszentrum Jülich GmbH, Institute of Energy and Climate Research, Materials Synthesis and Processing (IEK-1), 52425 Jülich, Germany
- 2 RWTH Aachen University, Institute of Mineral Engineering, 52064 Aachen, Germany
- 3 Forschungszentrum Jülich GmbH, Ernst Ruska-Centre for Microscopy and Spectroscopy with Electrons, Materials Science and Technology (ER-C 2), 52425 Jülich, Germany
- 4 Central Facility for Electron Microscopy (GFE), RWTH Aachen University, 52064 Aachen, Germany
- 5 Ruhr University Bochum, Institute for Experimental Physics II, 44801 Bochum, Germany
- 6 Heraeus Noblelight GmbH, 63450 Hanau, Germany
- 7 Forschungszentrum Jülich GmbH, Institute of Energy and Climate Research, Fundamental Electrochemistry (IEK-9), 52425, Jülich, Germany
- 8 RWTH Aachen University, Institute of Physical Chemistry, 52074 Aachen, Germany
- 9 Jülich Aachen Research Alliance, JARA-Energy, 52425, Jülich, Germany

# Correspondence

Christian Stern, Forschungszentrum Jülich GmbH, Institute of Energy and Climate Research, 52425,

Jülich, Germany. Email: <a href="mailto:c.stern@fz-juelich.de">c.stern@fz-juelich.de</a>

# **ABSTRACT**

Plasma etching is a crucial step in semiconductor manufacturing. High cleanliness and wafer-to-wafer reproducibility in the etching chamber are essential in order to successfully achieve nanometer-sized integrated functions on the wafer. The trend towards the application of more aggressive plasma compositions leads to higher demands on the plasma resistance of the materials used in the etching chamber. Due to its excellent etch resistance yttrium aluminum garnet  $Y_3AI_5O_{12}$  (YAG) is starting to replace established materials like SiO<sub>2</sub> or Al<sub>2</sub>O<sub>3</sub> in this kind of application. In this study reactive spark plasma sintering (SPS) was used to manufacture highly dense YAG ceramics from the respective oxides. In addition, yttrium was replaced with heavier lanthanoids (Er, Lu), intending to investigate the role of the A-site cation in the garnet type structure on the plasma erosion behavior. The produced materials were exposed to fluorine based etching plasmas mimicking the conditions in the semiconductor manufacturing apparatus and the erosion behavior was characterized by AFM, SIMS, TEM and surface profilers. The induced chemical gradient in the samples is limited to a few nanometers below the surface, which makes its characterization challenging. For advanced analysis, we developed a correlative characterization method combining SIMS and STEM-EDS enabling us to examine the structural and chemical changes in the reaction layer locally resolved. In the case of lanthanoid aluminates, an altered reaction layer and reduced fluorine penetration compared to YAG were found. However, a correlation between the characteristics of the induced chemical gradient and the determined etch rates was not evident.

#### 1. Introduction

The manufacturing of a silicon wafer is a complex process. In general, it can be divided into three different steps: patterning, etching and doping. The most common etching technique involves applying a plasma (an ionized gas) to the wafer. This technique is a combination of physical sputtering, hence accelerated ions bombarding the wafer, and chemical etching. For more information on the

fundamentals of semiconductor processing, we refer to the respective literature.<sup>1</sup>

Nowadays, continuous downsizing of the integrated circuits on the wafers requires more aggressive plasma compositions and leads to higher demand on cleanliness during the etching process. In order to achieve profitable production yields, process drifts and the formation of impurity particles need to be avoided at all cost. Conventional materials for inner wall components in plasma etching applications, such as quartz glass ( $SiO_2$ ) and alumina ( $Al_2O_3$ ), are prone to erosion when in contact with aggressive high-density fluorine plasmas. 2,3 While the reaction products of SiO2 are volatile, in the case of Al<sub>2</sub>O<sub>3</sub> reactions with the fluorine species cause the formation of impurity particles released into the semiconductor manufacturing apparatus, inducing wafer contamination.<sup>4,5</sup> For this reason, there is a need for the implementation of new advanced ceramics with enhanced plasma resistance. By replacing alumina with yttria, the inner wall erosion and particle generation can be significantly reduced. This can be explained by the higher formation enthalpy of yttria and the thermally more stable reaction products formed with the fluorine based etching plasma. <sup>6-9</sup> Recently, yttrium aluminum garnet (YAG) has been recognized as another promising inner wall material for plasma etching chambers. First patents on semiconductor manufacturing devices with components based on YAG were reported in the late 2000s. 10, 11 Kim et al. 12 and Qin et al. 5 studied the erosion behavior of YAG in fluorine based etching plasmas in 2011 and 2012. Both used commercially available Al<sub>2</sub>O<sub>3</sub> and Y<sub>2</sub>O<sub>3</sub> powders as starting materials to synthesize YAG via reactive sintering of pressed compacts using vacuum furnaces. After etching in CF<sub>4</sub>-based plasma, the erosion depth was determined using surface profilers. The results reveal excellent plasma resistance and erosion rates similar to yttria while YAG is available at a lower cost and has better mechanical properties.

With respect to the literature, the erosion of polycrystalline ceramics in fluorine-based plasmas is described as a physiochemical process comprehending two overlapping effects. On the one hand, the surface becomes chemically degraded driven by reactive plasma species such as CF<sub>4</sub>. On the other hand, material is physically removed by ion sputtering. Depending on the experimental parameters, the overall erosion can be more physically or chemically driven, making a clear allocation difficult.

In the past, the erosion process of ceramics in fluorine-based etching plasmas has been investigated by various characterization techniques. The surface topography is mainly studied using atomic force microscopy (AFM), profilometers or scanning electron microscopy (SEM). Secondary ion mass spectrometry (SIMS), X-ray photoelectron spectroscopy (XPS) and transmission electron microscopy (TEM) have been used to investigate the induced chemical gradients.<sup>5, 12-14</sup>

Until today, results about plasma etching of YAG in the literature are rare and mainly focus on the physical erosion. The formation of the reaction layer is limited to the surface and does not reach deep into the bulk, which makes the characterization challenging. In a previous study on yttria, a TEM analysis reveals a thickness of the reaction layer of around 10 nm after plasma exposure for 2 h.<sup>13</sup> To the best of our knowledge, a comparable in-depth investigation of the reaction layer for YAG is not available until now. For this reason, the general understanding of the plasma-material interaction is still sparse.

In this study, we aim to establish a novel approach to characterize the plasma-induced chemical gradient of highly etch resistant ceramics by correlating chemical information from SIMS and structural information from (S)TEM-EDS. For proof of our concept, YAG is used as a benchmark material and plasma parameters were chosen the same as in a previous study on yttria, where a mixed physiochemical degradation was observed.<sup>13, 14</sup> Replacing the yttrium ion (Y<sup>3+</sup>) in the garnet crystal by lanthanoids (Lu, Er) enables us to investigate the role of the A-site cations on the plasma-material interaction, aiming for enhanced plasma resistance.

Furthermore, we investigated whether characteristic values derived from the induced chemical gradient can be used to predict the plasma etch resistance. It is hypothesized that the substitution with heavier lanthanoid ions results in reduced plasma erosion and accordingly higher etch resistance. To minimize the influence of residual porosity on the plasma-material interaction, we applied a field-assisted sintering technology/ spark plasma sintering (FAST/SPS) process to synthesize samples with a minimum amount of residual porosity in a single consolidation step.<sup>15</sup> FAST/SPS is a densification technique that uses direct heating of the FAST/SPS tool through a pulsed direct current (DC) and

mechanical pressure at the same time. Therefore, shorter processing cycles and higher energy efficiency can be realized.<sup>16, 17</sup>

#### **Experimental procedure**

#### **Starting Materials**

In the present work, all aluminates have been synthesized by reactive FAST/SPS of the respective oxides. Commercial high purity  $Al_2O_3$  (A1 grade, 99.999 % purity,  $d_{50}$  = 1.1  $\mu$ m, Heraeus Holding GmbH) and  $Y_2O_3$  (99.999 % purity,  $d_{50}$  = 6.0  $\mu$ m, Neo Performance Materials Inc.) powders were used as raw materials to synthesize YAG ( $Y_3Al_5O_{12}$ ). By replacing  $Y_2O_3$  with  $Er_2O_3$  ( $d_{50}$  = 7.6  $\mu$ m) and  $Er_2O_3$  ( $d_{50}$  = 4.6  $\mu$ m) (both: 99.99 % purity, Neo Performance Materials) the alternative lanthanoid aluminates  $Er_3O_3$  ( $Er_3Al_5O_{12}$ ) and  $Er_3O_3O_3$  were created. The purity of the starting powders was confirmed using inductively coupled plasma (ICP) mass spectrometry (ICP-MS; Agilent Technologies 7900, USA). The major impurities in the alumina powder are traces of 0.1 ppm V, 0.1 ppm Mn, 0.1 ppm Ni and 0.8 ppm Cu. The yttria powder contains traces of 0.1 ppm Li, 0.3 ppm Na, 0.8 ppm Fe, 0.1 ppm Ba and less than 2 ppm of lanthanoids. The major impurities in the lanthanoid oxides are Sr, Rb, Al and other lanthanoid elements in the ppm level. The particle size distributions (PSD) were determined with a LA950 V2 particle size analyzer (Horiba, Kyoto, Japan) and are summarized in the supplementary information (Figure S1).

#### **Processing**

The raw materials were weighed according to stoichiometry, creating batches of 250 g of each powder. The same amount of alumina grinding balls ( $\emptyset$  10 mm) and 0.4 L of ethanol were added to form a slurry. After homogenization for 24 h on a roller bench, the slurry was dried using a rotary evaporator. After a subsequent sieving step (90  $\mu$ m mesh), the powder was calcined for 3.5 h at 1000 °C, followed by another sieving step (90  $\mu$ m mesh).

#### Reactive spark plasma sintering of Y and RE garnets

All of the aluminum garnets investigated in this study have been synthesized by reactive FAST/SPS of the respective oxides. The chemical reaction to form YAG from alumina and yttria is described as follows:<sup>18</sup>

$$3 Y_2 O_3 + 5 Al_2 O_3 \rightarrow 2 Y_3 Al_5 O_{12}$$
 (YAG) (1.1)

The formation of the lanthanoid compounds follows an identical reaction, where Y is substituted by the corresponding rare earth cation (Er³+ or Lu³+). By using reactive FAST/SPS, we can avoid sintering additives and high temperatures which are conventionally used when synthesizing YAG.¹9 Here, a DSC50 (Thermal Technology LLC, NV, USA) FAST/SPS device was used to press 40 mm disks using a graphite die. Following a pre-compaction step with 20 MPa, the powders were heated at a heating rate of 25 K/min to 1000 °C and then at a heating rate of 10 K/min to 1625 °C while uniaxial pressure of 5 MPa and 25 MPa was applied during the respective heating steps. Heating was followed by a 30 min dwell at 1625 °C with 25 MPa pressure. Afterwards, the SPS system was switched to active cooling mode. The FAST/SPS parameters are summarized in Fig. 1.

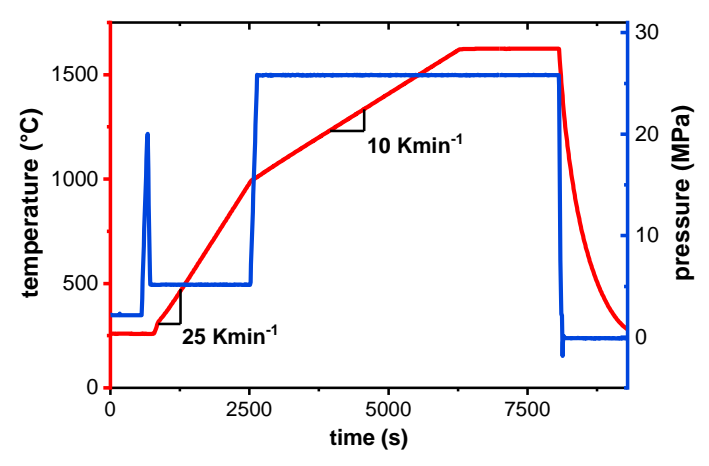


Fig. 1. Parameters for the reactive spark plasma sintering of YAG, ErAG and LuAG.

#### Plasma etching experiments

For plasma etching, the samples were cut in squares (10 mm x 10 mm) and the thickness was reduced below 1 mm by grinding and polishing. The last polishing step was done using colloidal silica in order to achieve a mirror-like finish and to eliminate defects that could influence the erosion process. Before the plasma exposure, all samples were half masked with plasma-resistant polyimide (Kapton®) tape to induce etch steps and enable measurement of an etch rate. The sample holder and half masked samples are shown in the supplementary Figure S2. A quartz glass (SiO<sub>2</sub>) reference sample was etched in each run to keep track of process drifts and ease comparability of the different runs.

The etch experiments were conducted in an inductively coupled plasma (ICP) plasma reactor using CF<sub>4</sub>, Ar and O<sub>2</sub> as plasma gases. Details on the experimental set up and working principle of the etch chamber can be found elsewhere.<sup>20</sup> The plasma parameters were chosen with respect to previous etching studies on yttria (Y<sub>2</sub>O<sub>3</sub>) by Kindelmann et al. that were carried out in the same etch chamber.<sup>14</sup>, In the first etch run, YAG and ErAG were etched at the same time. In the second etch run with the LuAG sample, plasma instabilities occurred requiring an adjustment of the plasma parameters that lead to a less aggressive plasma gas composition. During the evaluation it became obvious that the plasma parameters were too weak to trigger physical erosion. For this reason, a third etch run with more aggressive etching conditions was conducted. Since the power of the ICP-generator (P<sub>ICP</sub>) could

not be further increased, we decided to decrease the chamber pressure and increase the bias voltage.

The plasma parameters are summarized in Table 1.

**Table 1** Parameters for etch experiments.

Samples	P <sub>ICP</sub>	t <sub>etch</sub>	p [mbar]	U <sub>B</sub> [V]	CF <sub>4</sub> [sccm]	Ar [sccm]	O <sub>2</sub> [sccm]
YAG, ErAG	600	120	0.02	-150	1.0	5.0	0.3
LuAG	600	120	0.02	-150	0.5	5.0	0.0
YAG, ErAG,	600	120	0.0083	-250	1.0	5.0	0.5
LuAG							

In yttria, Kindelmann et al observed a shift of the dominating plasma erosion mechanisms depending on the plasma parameters.<sup>13</sup> In our study we assume that the adapted plasma parameters changed these mechanisms from being more chemically driven to more physically driven.

# Characterization of starting materials and plasma-material interaction

For characterization of the microstructure after reactive spark plasma sintering, the samples were ceramographically ground and polished. Scanning electron microscopy (SEM, Ultra 55, Carl Zeiss AG, Germany) was used to analyze the microstructure.

After the plasma treatment, different characterization techniques were combined to characterize the surface and the reaction layer. Atomic force microscopy (AFM, Bruker Dimension Icon, USA) was used to investigate the surface topography. Tapping mode was used for the measurements and as cantilevers PPP-NCHR (NANOSENSORS, tip radius of curvature < 10 nm) with Al-coating on detector side and a nominal spring constant of 10 - 130 N/m have been used as received and calibrated

individually. The results were evaluated using the software package Gwyddion (Version 2.61). Measurement artefacts like scars and strokes were removed and suitable background functions were applied to achieve comparable results.

The physical erosion of the samples etched in the third etch run was evaluated using a surface profilometer (Dektak 6M, Veeco, NY, USA). The step height was averaged from 4 line scans.

The induced chemical gradient that has been formed due to the plasma treatment was analyzed by means of time-of-flight secondary ion mass spectrometry (TOF-SIMS 5 NCS system, ION-TOF GmbH, Germany). A Bi $^+$  liquid metal ion gun was used as primary ion source operating at an energy of 30 keV and a raster size of 50  $\mu$ m  $\times$  50  $\mu$ m at a resolution of 128  $\times$  128 pixels. Cs $^+$  ions were used as sputter ions at an energy of 1 keV in a 250  $\mu$ m  $\times$  250  $\mu$ m raster. Charge compensation was accomplished by a low-energy electron flood gun and Ar main flooding at a pressure of 2·10-6 mbar. Spectra were taken in positive and negative polarity in spectrometry mode. Crater depth were measured on the on-device attached AFM of the NCS system in contact mode. ToF-SIMS sputter times were linearly converted into a depth scale obtained from AFM measurements.

Furthermore, transmission electron microscopy (TEM, JEM F200, JEOL Ltd., Japan) was used to resolve the reaction layer at the surface. High-resolution TEM (HRTEM) was used to depict the crystal structure and potential damage caused by Ar<sup>+</sup> sputtering during the plasma treatment. Additionally, energy dispersive spectroscopy (EDS) measurements using a scanning TEM (STEM) enable the characterization of the induced chemical gradients. All lamellae were extracted from a representative surface area using focused ion beam machining (FIB, FEI Strata 400, USA).

#### 2. Results and discussion

#### Microstructure and phase composition

Secondary electron SEM images of samples after reactive FAST/SPS sintering in the as-sintered state are shown in Figure 2. YAG (Fig. 2 (A-B)) was thermally etched at 1250 °C and ErAG (Fig. 2(D)) and LuAG (Fig. 2(F)) at 1200 °C for 30 min in order to make grain boundaries visible and get a clearer picture of the microstructure. In general, the samples are dense and homogenous, even though scattered pores are visible at triple points (Fig. 2(A) and (F)). The most apparent difference between the materials is the amount of a dark secondary phase. The secondary phase can clearly be identified as alumina in the SEM/EDS analysis of the etch step in the supplementary information (Figure S3).

The amount of excess alumina differs from being almost negligible in YAG, the appearance of scattered clusters in LuAG to a phase volume fraction of about 4 % in ErAG. Possible reasons for this behavior are inaccuracies during the powder processing, differences in the alumina incorporation during homogenization or different loss on ignition (LOI) values during sintering. YAG is a line compound and therefore its phase pure synthesis is challenging.<sup>22</sup> The effects of non-stoichiometry on the phase evolution are complex and are considered out of scope of this study.

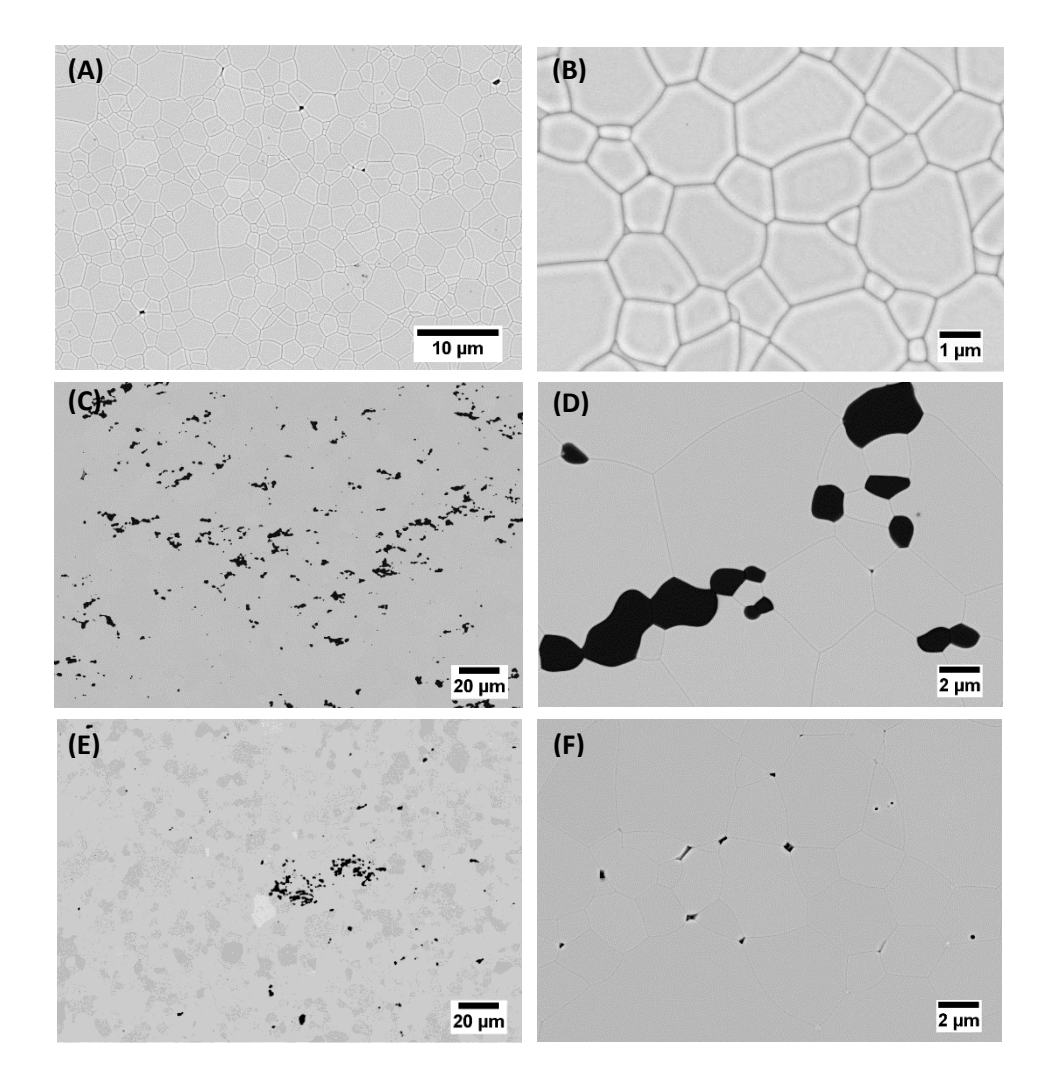


Fig. 2. SEM of samples after sintering. (A-B) YAG. (C-D) ErAG. (E-F) LuAG.

## Surface topography and erosion behavior

Plasma etching is a very sensitive process and small changes in the experimental parameters can have a significant impact on the results. To allow comparability of the different etch runs, one quartz glass  $(SiO_2)$  reference sample was half masked and etched in every run. After etching, the erosion depth of the reference sample was determined with a laser microscope (VK-9710 Keyence Corporation, Japan). The results in Table 2 indicate that the lower  $CF_4$  and  $O_2$  content in the second etch run (Table 1) resulted in a significantly reduced erosion depth of the quartz glass reference sample. A possible reason for this behavior is the decreased amount of the chemically reactive species ( $CF_4$ ) which leads to a smaller contribution of chemically driven erosion. Another reason could be the plasma instabilities requiring the gas composition to be adjusted in the second etch run.

In the third etch run the increase in bias voltage and decrease in chamber pressure lead to a significantly more aggressive plasma and an erosion depth of  $8.5~\mu m$  in the reference sample.

**Table 2** Overview of the conducted etch runs and erosion depth of reference samples determined by laser microscope.

Run		Samples			Erosion depth of SiO <sub>2</sub>
					reference sample (μm)
1	YAG	ErAG		SiO <sub>2</sub>	3.3
2	LuAG			SiO <sub>2</sub>	0.7
3	YAG	ErAG	LuAG	SiO <sub>2</sub>	8.5

To better understand the influence of the A-site ion in the garnet type structure on the etch performance, the induced etch steps in the transition zone from the etched to the shielded surface were analyzed by means of AFM. Figure 3 summarizes the results. All garnet samples did not show a well pronounced etch step, but a contamination covering the latter. Even after multiple cleaning steps with acetone, the contamination was still present. Therefore, the respective surface area was analyzed by means of SEM/EDS. The results are summarized in the supplementary information (Figure S3) and

indicate a surface contamination with metal ions, namely Fe and Ni. In the test reactor, the plasma interaction is not limited to the sample surface but happens in the whole chamber. The metal ions presumably originate from the chamber wall or sample holder, which are made of stainless steel <sup>20</sup>. The local differences in surface topography at the fringe of the polyimide tape result in a disturbed gas flow and therefore local differences in the plasma gas composition. This effect might induce the predominant re-deposition of metal ions near the etch step, making a direct measurement of the erosion depth for YAG and LuAG (Figure 3 (A) and (B)) very challenging.

A surface treatment was not undertaken in order to preserve the as-etched status of the samples. Since the contamination is least pronounced in the ErAG sample, the topography at the etch step could still be analyzed. The black features in the etched area in ErAG (Fig. 3 (C), white arrows) represent the former alumina secondary phase, that was predominantly eroded. It is stated in the literature that alumina has a lower plasma resistance than yttria and thereby a lower plasma resistance than YAG, LuAG and ErAG. The line scans in Fig. 3 (D) show that there is almost no height difference between the etched and unetched side. This indicates that under the given conditions only minor physical erosion took place. In contrast, in previous studies on yttria, a significant amount of physical erosion was already found under comparable conditions in the same etch chamber. This leads to the assumption that the materials investigated in the present study have a better plasma resistance than yttria. However, further plasma tests with harsher conditions and exchanging SiO<sub>2</sub> reference with Y<sub>2</sub>O<sub>3</sub> reference are required to reliably benchmark these materials.

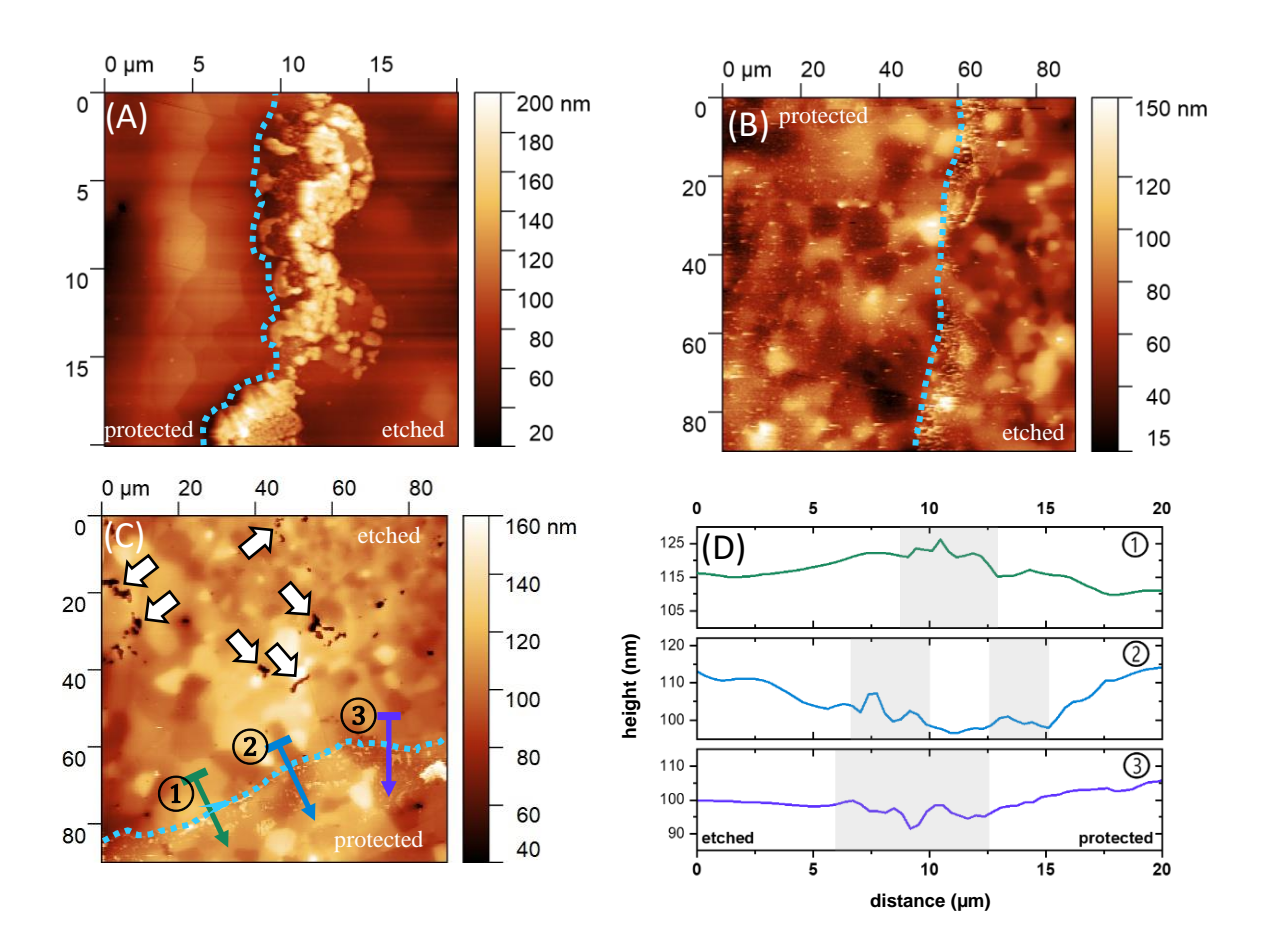


Fig. 3. AFM images of transition from etched to protected surface. (A) YAG (B) LuAG (C) ErAG (D) Corresponding line-scans to (C). Dashed blue lines indicate location of etch step. White arrows in Fig. 3 (C) highlight former alumina phase and gray shaded areas in Fig 3 (D) indicate contamination.

## Characterization of the reaction layer by ToF-SIMS

Even though the plasma power during the first etch run was too low to trigger detectable physical erosion, the plasma still induces chemical changes at the surface of the samples. To get a better understanding of the formed reaction layer, the etched samples were examined by means of time-of-flight secondary ion mass spectrometry (ToF-SIMS). Typically, for group 5, 6 and 7 elements as well as carbon and hydrogen the yield of negative species in negative polarity of ToF-SIMS is higher than their respective yield as positive species in positive polarity.<sup>24</sup> The fluorination is the most prominent induced change in chemistry observed and fluorine is a group 7 element. Therefore, the measurements in negative polarity are preferentially used to characterize the reaction layer. The following figure shows the depth profiles of the negative species for all investigated materials as well as the depth profile of the positive species in case of YAG (Figure 4 (A-B)). Assuming constant sputter rates, the time scale of SIMS was converted to a depth scale. The

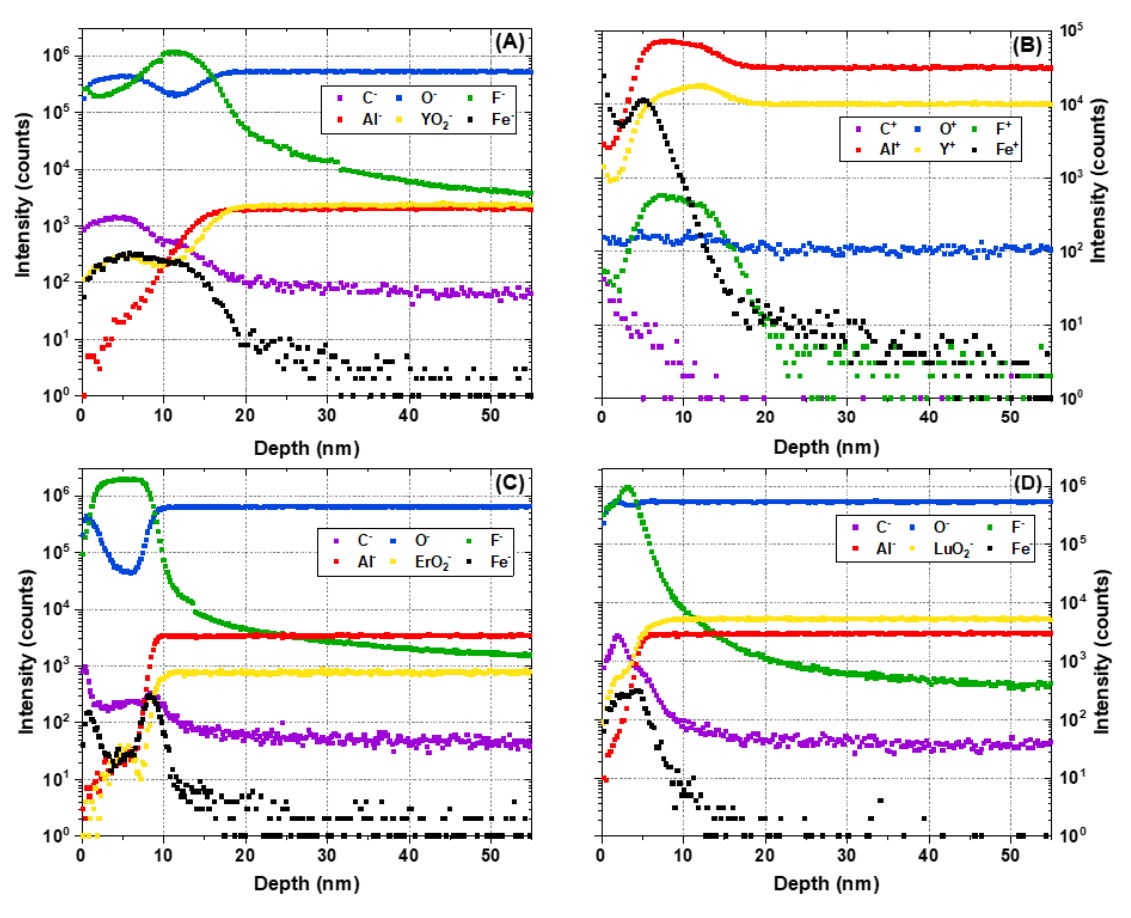


Fig. 4. Time-of-flight secondary ion mass spectrometry (ToF-SIMS) depth profiles of all samples after plasma etching. (A) YAG (negative polarity) (B) YAG (positive polarity) (C) ErAG (negative polarity) (D) LuAG (negative polarity).

results of the underlying AFM measurements are summarized in Table 3. The holes caused by the preferentially eroded alumina phase (Figure 3(C)) are a possible explanation for the differences in surface roughness ( $R_a$ ). Unfortunately, high  $R_a$  values compared to the measured crater depth complicates the evaluation and is an important source of error.

**Table 3** Surface roughness  $R_a$  and depth of SIMS crater measured by the on device attached AFM.

	Depth of crater(nm)	R <sub>a</sub> (nm)
YAG	56	20
ErAG	97.5	47
LuAG	172	62

In all samples, a reaction layer with altered chemical composition compared to the bulk was found. The positive and negative measurements of YAG (Figure 4(A-B)) illustrate the different intensities of the respective elements (except Y-species) depending on the polarity of the measurement. The fluorine and oxygen yield in the negative measurement (Figure 4(A)) exceed the yield in the positive measurement (Figure 4(B)). Vice versa the aluminum, yttrium and iron yields in positive polarity exceed the yield negative polarity.

An assessment of critical parameters in the reaction layer has not yet been established in the literature. A possible approach is comparing the thickness of the reaction layer. However, the literature currently lacks a definition of the limits of this reaction layer. Therefore, it was decided to define the lower bound by estimating the depth at which the bulk ions reach a constant intensity. This approach results in an estimated thickness of 18 nm for YAG, 10 nm for ErAG and 6 nm for LuAG, respectively. The reduced extent of the reaction layer hints on an enhanced chemical stability against the plasma of the erbium aluminate when comparing YAG and ErAG. In LuAG, the reaction layer is even less pronounced. But in this case, a direct comparison to YAG and ErAG is not feasible since the samples were etched in different runs with the second being less aggressive (Table 2). run

Another possible value to compare the etch resistance based on the chemical gradient is the fluorination depth. This value was assessed by calculating the inflection point of the fluorine intensity using OriginPro 2020. The calculated values of 17.5 nm for YAG, 9.4 nm for ErAG and 5.3 nm for LuAG are only slightly deviating from the assessed thickness.

Within the reaction layer, a variation of the fluorine content is observed for all samples. This variation is characterized by a maximum of fluorine intensity close to the surface and a lower intensity zone reaching deeper into the bulk. Similar results were observed by Kindelmann et al. in a study on the etch resistance of yttria. <sup>14</sup> In this study the fluorine peak is reached in a depth of 10 nm in YAG, 2 nm in ErAG and 3 nm in LuAG. The maximum of the fluorine intensity coincides with a depletion of oxygen ions that is particularly pronounced in ErAG. A possible explanation for this is that fluorine ions occupy oxygen sites in the garnet crystal. However, subsequent TEM observations suggest that the reaction layer is mostly amorphous. Furthermore, high C<sup>-</sup> and Fe<sup>-</sup> concentrations were detected in the reaction layer. The presence of C<sup>-</sup> can be attributed to the degradation of CF<sub>4</sub> molecules that adsorbed on the surface, whereas the Fe<sup>-</sup> ions have been eroded from metallic components in the etch chamber. In contrast to the course of Fe<sup>-</sup> and C<sup>-</sup> ions, which mainly appear in the reaction layer, fluorine penetrates deeper into the bulk of the samples. This phenomenon is especially visible in YAG, whereas in ErAG and LuAG the F<sup>-</sup> intensity drops more significantly at the interface between reaction layer and bulk. Here, the higher atomic mass of Er and Lu when compared to Y might have an influence on the penetration depth.

To confirm that the induced chemical gradient is a consequence of interaction with the fluorine based etching plasma an as sintered reference sample has been grinded, polished and analyzed by ToF-SIMS. The results in appendix (Figure S4) indicate altered chemical composition on the sample surface up to a depth of less than 5 nm. This can be attributed to the diamond suspension and epoxy resin that was used for the sample preparation. However, deeper into the bulk the intensities of all ions are constant. Furthermore, ToF-SIMS was also employed for the characterization of the physically eroded samples.

The results suggest that due to the continuous erosion no reaction layer could form. The only

detectable impact of the plasma is fluorination and iron implantation reaching roughly 5 nm into the sample.

#### Characterization of the reaction layer by HRTEM and (S)TEM-EDS

In order to verify the thickness of the reaction layer and to support the depth-resolved SIMS measurements of the different elements, FIB lamellae have been prepared and analyzed by means of TEM and STEM-EDS. For the lamella preparation using focused ion beam machining (FIB) the samples were coated with graphite and platinum. Figure 5 shows an example of the cross section of the reaction zone in YAG and LuAG in the HRTEM mode. For ErAG, no HRTEM image could be acquired. Below the graphite and platinum coating, the TEM images of YAG and LuAG show an amorphous surface layer of roughly 20 nm in YAG and 9 nm in LuAG (marked with white arrows in Fig. 5, a scattering of several nm is obvious). The physical damage of the garnet crystal resulting in the amorphous layer can be explained by the Ar<sup>+</sup> sputtering. The extent of the amorphous zone corresponds to a good extent with the thickness of the reaction layer determined by the respective SIMS measurements (18 nm for YAG and 6 nm for LuAG). Nevertheless, we can only assume whether the whole reaction layer is amorphous or whether the altered chemical composition reaches deeper into the bulk.

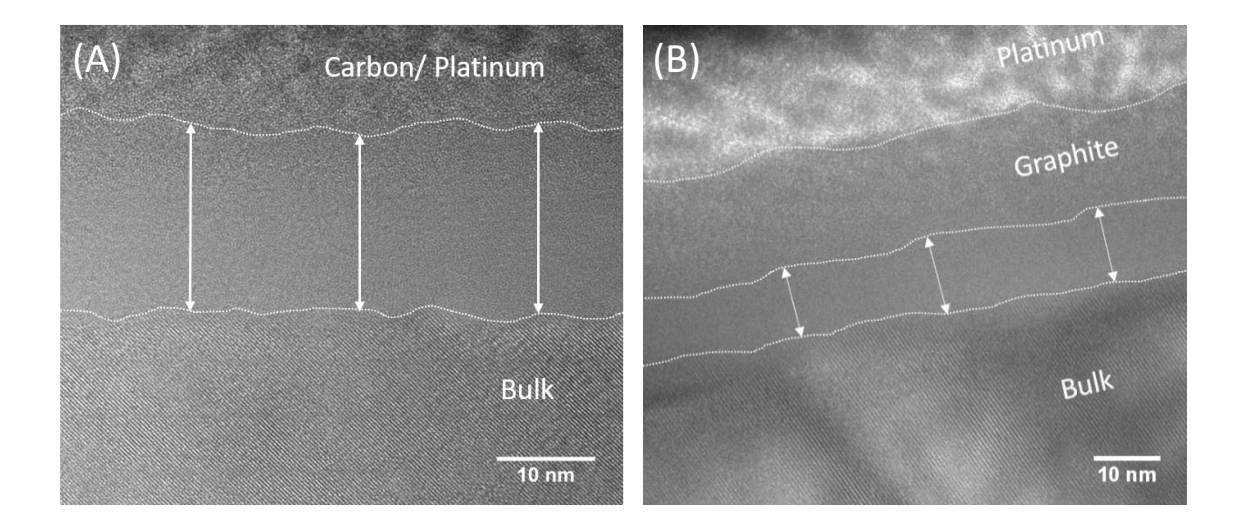


Fig. 5. HRTEM image of (A) YAG and (B) LuAG after plasma exposure for 2 h. White arrows illustrate the extent of the physically damaged surface zone.

The induced chemical gradient was also examined by means of STEM-EDS. Fig. 6 shows the integrated intensities of the relevant elements in the reaction layer after plasma exposure. The corresponding EDS mappings can be found in the supplementary information (Figures S6-8). The graphs can be divided into three distinct parts: 1) The graphite and platinum coating that was applied for the FIB preparation; 2) The reaction layer induced by the plasma material interaction; and 3) The bulk which is unaltered besides for the fluorination. The transition between the three parts is not clearly defined but rather merging into one another.

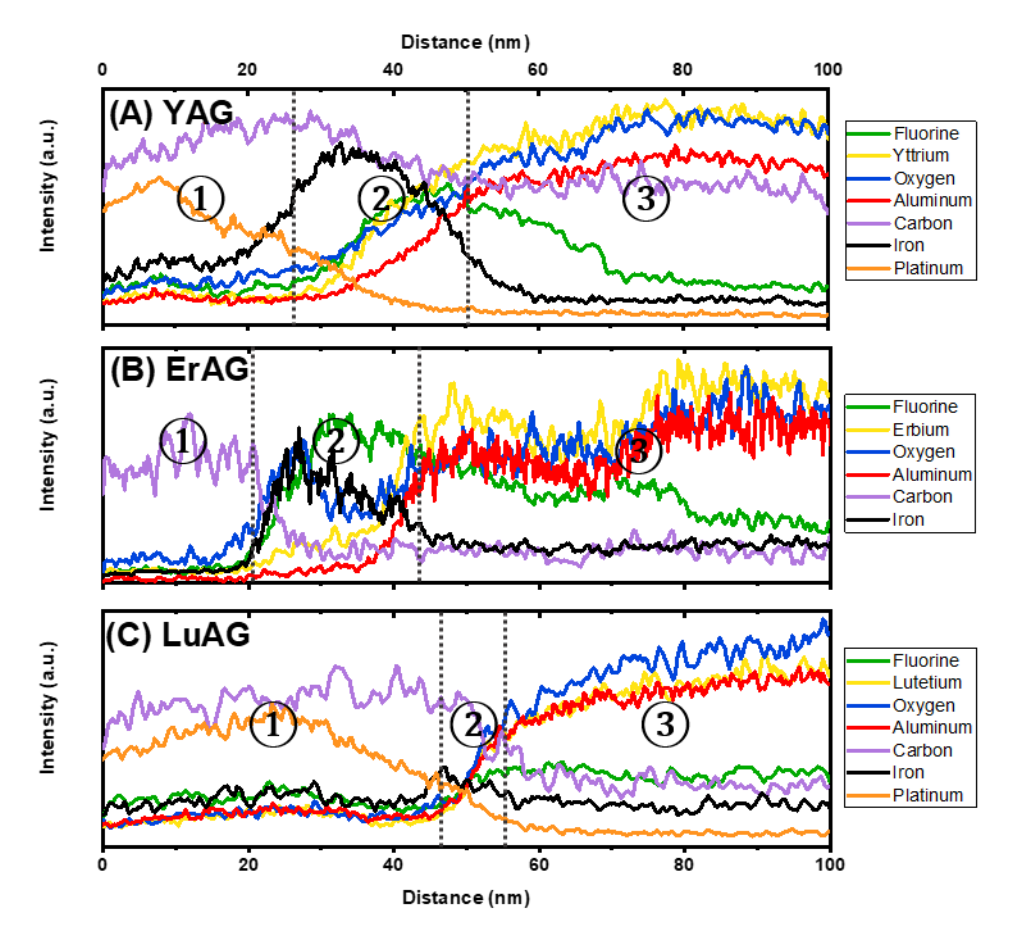


Fig. 6. Integrated intensities acquired form STEM-EDS of (A) YAG (B) ErAG and (C) LuAG after plasma exposure for 2h. 1 Platinum/ Graphite. 2 Reaction layer. 3 Bulk.

The high Pt and C intensities on the left side of the graphs are attributed to the conductive Pt/C coating. Because of the thickness of the C coating on the ErAG sample, the applied Pt layer was out of the measuring range, and therefore no signal is available. The increase in Fe and decrease in Pt intensity indicate the transition towards the sample surface. From the processing side, the presence of Pt in the reaction layer and Fe in the coating in YAG (Fig. 7(A)) can be excluded. Nevertheless, they are measured in the transition zone, which might be caused by localized thickness variations of the respective layers

or a non-ideal (non-perpendicular) sample orientation in the analyzed area.

The reaction layer is characterized by an increase of the intensities of the bulk ions (Al, O, Y/Er/Lu) and F. In YAG and LuAG the bulk ion signals slowly increase over the whole reaction layer, whereas in ErAG the intensities stay on a low level before they start to increase at the interface towards the unaltered bulk. The fluorination is most pronounced in ErAG and negligible in LuAG. In ErAG, the maximum of the fluorine intensity coincides with an oxygen depletion and is reached earlier compared to YAG. In all samples the Fe intensity in the reaction layer increases, reaches a maximum after a few nanometers and decreases again when approaching the bulk of the samples. The course of the C intensity differs in the three samples. A slight but continuous decrease was observed in YAG. After a significant drop at the beginning of the reaction layer in ErAG, the intensity continues to decrease and reaches a constant level in the middle of the reaction layer. In LuAG and YAG, the course of the intensity is comparable as the intensity decreases throughout the reaction layer and attains at a constant level in the bulk. A possible explanation for the higher C intensities at the top of the reaction layer is the formation of a fluorocarbon polymer on the surface, as described by Miwa et al.8 However, oxygen was intentionally added to inhibit the formation of such a polymer layer as it was described in the literature before.<sup>25</sup> Therefore, the presence of fluorocarbon polymer in the reaction layer is unlikely but cannot be excluded based on the acquired data.

The interface between reaction layer and bulk can be estimated by the Fe signal approaching zero and the bulk ions (AI, Y/Er/Lu, O) reach a constant level. Again, the exact position of the interface can only be estimated. Except for the fluorination, no chemical changes could be observed in the bulk of the sample.

Compared to the YAG and ErAG samples, LuAG is the least altered. A possible explanation for this behavior is the comparatively less aggressive etching environment during the second etch run (Table 2).

#### **Correlative characterization**

ToF-SIMS and STEM-EDS enable the characterization of the induced chemical gradient, even though the information is generated in different ways. In ToF-SIMS, ions are detected by a mass spectrometer, whereas STEM-EDS uses characteristic X-rays to determine the intensities. <sup>26, 27</sup> With the purpose of verifying the results achieved, the following section discusses the correlation of the STEM-EDS and ToF-SIMS analysis results. The yield of positive or negative species in ToF-SIMS depends on the element and the respective polarity of the measurement. For the correlation of SIMS and TEM, alternative SIMS graphs, showing positive or negative species of their respective measurement polarity giving a higher yield were created. F, O and C were taken from negative polarity measurements, whereas AI, Y, Fe and lanthanoids were taken from measurements in positive polarity. Since SIMS does not require a conductive coating, depth profiles start at the actual sample surface. Therefore, the interface between coating and sample in STEM-EDS has been used for depth correlation by bringing this interface and the zero-position of the ToF-SIMS measurement in coincidence. Please note, that the exact position of the interface can only be assumed. For the correlation, the interface was set to the same positions as in Fig. 6 (dashed lines).

The correlated results of the STEM-EDS and ToF-SIMS results in YAG are shown in Figure 7. Both graphs show the same trends and especially the Fe and C intensities are in good agreement. In both measurements, the fluorine intensity rises with increasing distance from the sample surface, before it reaches a maximum towards the lower bound of the reaction layer. This maximum is reached in a lower depth in the SIMS measurement. Furthermore, the bulk ions (AI $^+$ , Y $^+$ , O $^-$ ) attain a constant level in a lower depth in SIMS compared to the STEM-EDS results. A possible explanation for this is that the ToF-SIMS data is averaged over the whole analysis area (50  $\mu$ m × 50  $\mu$ m), whereas the STEM results are acquired on a nanometer sized area. Furthermore, the STEM and the SIMS measurements were carried out at different parts of the sample. Another factor is the complicated depth measurement of the SIMS crater and the subsequent calculation of the sputter rate. Nevertheless, qualitative effects of plasma etching and reaction layers are well in agreement between the different methods and allow for further investigation.

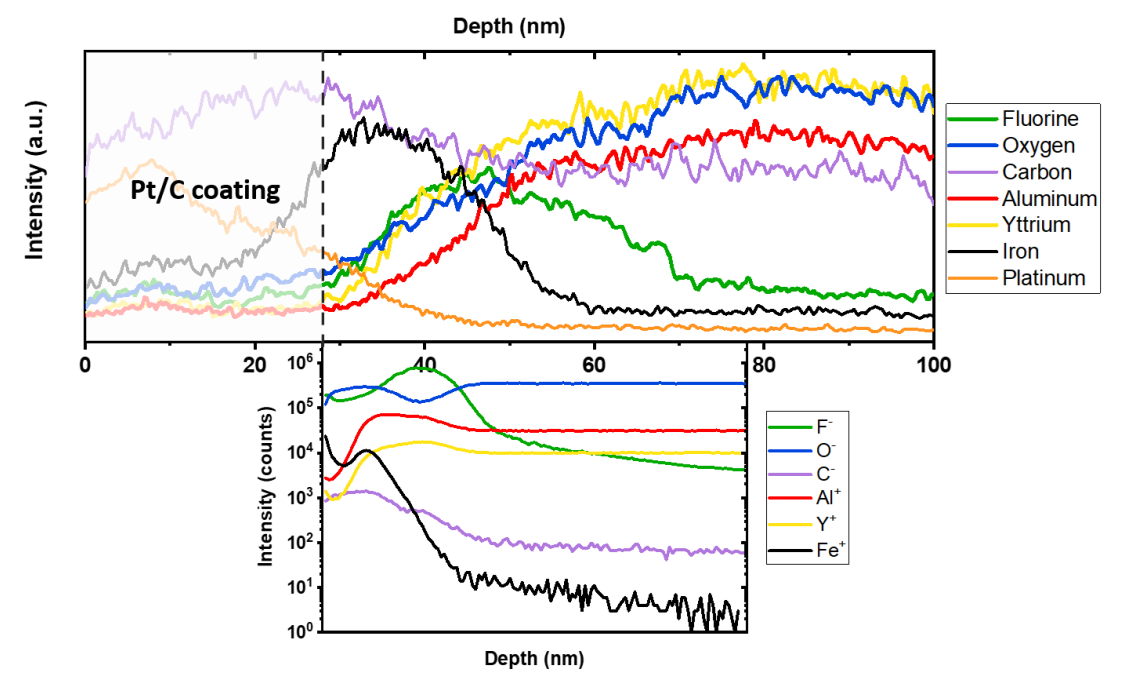


Fig. 7. Induced chemical gradient in YAG. Correlation of STEM-EDS (top) and ToF-SIMS (bottom).

The same characterization procedure was applied to ErAG. The results in Figure 8 are comparable to the results for YAG (Figure 7). Here it has to be mentioned that the positive measurement of ToF-SIMS was stopped after reaching a sputter depth of roughly 33 nm. Therefore, the Al<sup>+</sup>, Er<sup>+</sup> and Fe<sup>+</sup> measurements in Figure 7 do not reach deeper into the bulk. In general, both graphs show the same trends. The fluorine maximum coincides with the oxygen depletion and the increase of the bulk ions (Al, Er) only occurs towards the lower bound of the reaction layer. In this case, the difference in scaling of both graphs is even more prominent. The thickness of the reaction layer in ToF-SIMS is only about half the size of the thickness in the STEM-EDS measurement. The reasons for this are the same as mentioned for YAG namely different measurement spots, the data being acquired more locally in STEM, and the complicated conversion of the depth scale in ToF-SIMS.

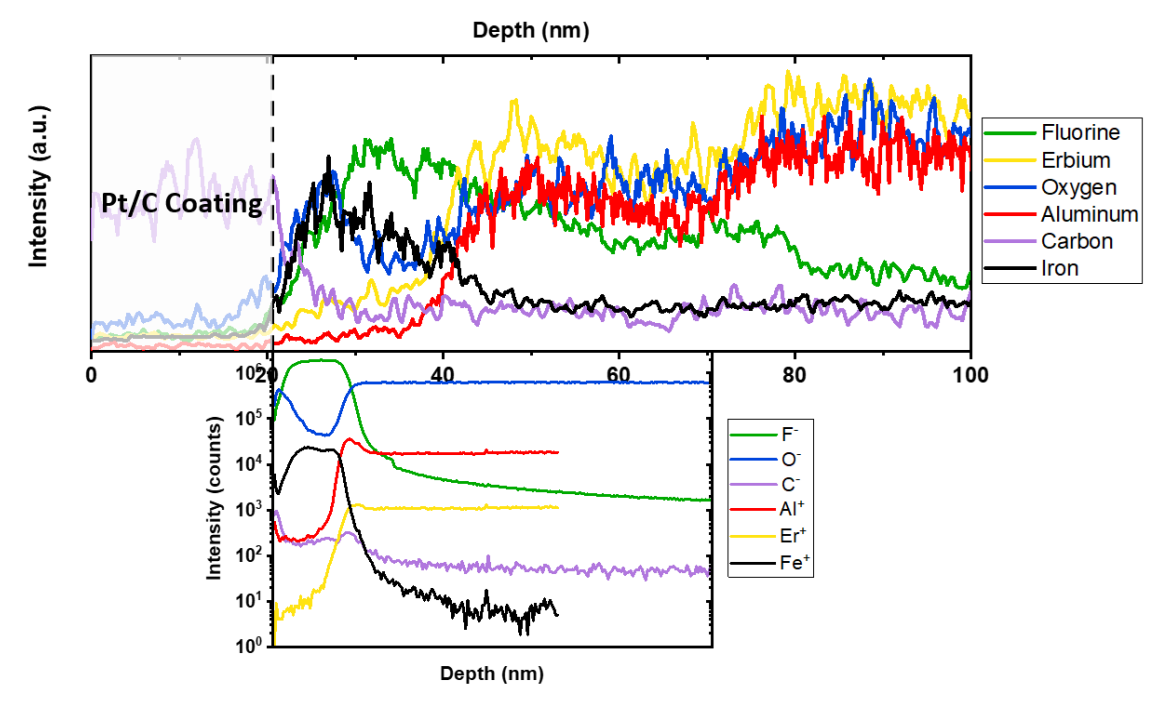


Fig. 8. Induced chemical gradient in ErAG. Correlation of STEM-EDS (top) and ToF-SIMS (bottom).

Finally, the characterization procedure was also applied on the LuAG sample. The results are summarized in Figure 9. As for YAG and ErAG, both graphs show the same trends and the intensities are in good agreement. Compared to the YAG and ErAG samples, the induced chemical gradient is least pronounced in LuAG. Due to the low intensities, the interpretation of the fluorine and iron signal in the STEM measurement is challenging. After the correlation, the extent of the fluorination and iron penetration can be assumed with high certainty. In this case, the interpretation of the scaling of both graphs is questionable. The overlapping of the Pt and Fe intensities impedes the positioning of the interface between coating and sample and as a consequence the correlation itself.

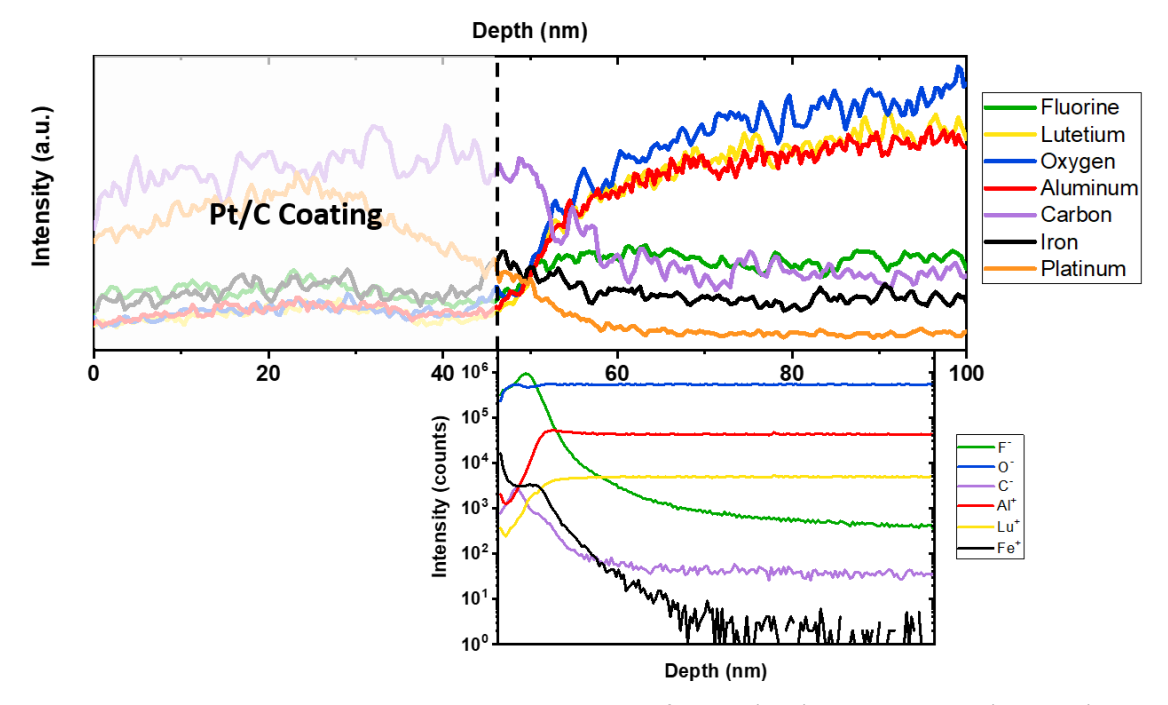


Fig. 9. Induced chemical gradient in LuAG. Correlation of STEM (top) and ToF-SIMS (bottom).

# **Physical erosion**

The adjusted plasma parameters (Table 1) lead to significant erosion of all samples. The determined erosion depth is shown in Table 4 and compared to the characteristic values that were derived during the analysis of the induced chemical gradient. The erosion depth of YAG and ErAG in the third etch run is almost equal. However, the thickness of the reaction layer as well as the fluorination depth after etching in less aggressive plasma conditions is significantly larger in YAG compared to ErAG. This result indicates that the induced chemical gradient can not be used to predict the resistance against plasma

erosion. Furthermore, the reaction layer neither has a passivating effect nor does a less pronounced reaction layer govern enhanced plasma resistance. Since LuAG was etched in a different run, its higher erosion depth must not be linked to the values derived from the induced chemical gradient.

Table 4. Characteristic values derived from ToF-SIMS and erosion depth determined with the surface profiler.

Material	Thickness of reaction layer (nm)	Fluorination depth (nm)	Erosion depth (nm) in aggressive run
YAG	18	17.5	406
ErAG	10	9.4	411
LuAG	6	5.3	551

#### 3. Conclusions

In the present study, various ceramics with garnet structure (YAG, ErAG, LuAG) have been successfully synthesized by means of reactive spark plasma sintering. SEM investigations indicate a dense, homogenous microstructure, even though excess alumina has been observed in different amounts. The results of the plasma etching study indicate that all samples have a high resistance against the fluorine based etching plasma. Our initial plasma parameters were too weak to trigger relevant physical erosion. Nevertheless, due to the interplay with the plasma a mostly amorphous reaction layer was found in all samples. Addition ally, a third etch run with more favorable plasma parameters was initiated that resulted in physical erosion of all samples.

Due to the absence of physical erosion in the 1<sup>st</sup> and 2<sup>nd</sup> etch run established characterization methods like surface profilers or AFM fail when benchmarking these materials regarding their etch resistance and evaluating the effect when replacing Y by lanthanoid elements. For this reason, an in-depth analysis of the induced chemical gradient was carried out and characteristic values such as the thickness of the reaction layer or the fluorination depth were derived. An assessment of the plasma resistance based on this gradient has not yet been established in the literature. For a better understanding we introduced – to our knowledge for the first time - the combination of SIMS and

(S)TEM/EDS as an alternative characterization strategy. A major advantage of SIMS is that depending on the element, the yield and thereby the intensity of the positive or negative polarity measurements are higher. This becomes especially advantageous when the intensities in STEM/EDS are comparatively low and hard to interpret. In the present study, the correlation enabled quantification of the fluorination in LuAG. Another challenge that became obvious in the present work is the appropriate scaling of the SIMS measurements. After the correlation, the scaling of the SIMS data tends to be compressed compared to the STEM results. By comparing the distribution of the same ions in SIMS and STEM, it would be possible to adjust the scaling. In other words: by correlating STEM-EDS with ToF-SIMS, the major drawbacks, being low intensities in STEM-EDS and challenging scaling in ToF-SIMS, can be overcome.

In the 3<sup>rd</sup> etch run all samples were physically eroded. The erosion depth indicates that the etch performance of YAG and ErAG is almost equal, whereas LuAG was eroded more. This is in contrast to the assessed values of the induced chemical gradient. This leads to the conclusion, that the chemical gradient cannot be used to assess the plasma resistance. Furthermore, the substitution of Y³+ with heavier lanthanoids did not result in enhanced plasma resistance which leads to the assumption, that the A-site cation is not critical with respect to the etch resistance. Nevertheless, all materials offer excellent plasma resistance and are potential candidates for the application in semiconductor manufacturing. The results also leave room for follow up studies using more accessible elements to substitute the yttrium ion in the garnet crystal. An in-depth investigation of the physical erosion of the samples etched in the last etch run will be carried out in a follow up study.

For further etch experiments, the experimental setup leaves still room for improvements. As a measure to overcome the issue of etch step contamination, it is recommended to avoid metallic surfaces in the etch chamber. Metallic components that come in contact with the plasma result in the observed contamination by iron and nickel. Since the manufacturing of ceramic components with complex geometries is rather difficult, ceramic coatings such as yttria or YAG on metallic components are a promising solution.

The observed fluctuations of the plasma lead to the conclusion that only samples that were etched in the same etch run can be compared with each other. For future experiments an adjusted sample holder that can hold more samples at a time would be beneficial.

# Acknowledgements

The authors acknowledge Sebastian Zischke for executing (S)TEM-EDS investigations and Doris Sebold for SEM/EDS characterizations.

#### **REFERENCES**

- 1. Mack C. Fundamental Principles of Optical Lithography: The Science of Microfabrication, London: John Wiley & Sons; 2007.
- 2. Leech PW. Reactive ion etching of quartz and silica-based glasses in CF4/CHF3 plasmas. Vacuum. 1999;55(3-4):191-96.
- 3. Kim D-M, Kim K-B, Yoon S-Y, Oh Y-S, Kim H-T, Lee S-M. Effects of artificial pores and purity on the erosion behaviors of polycrystalline Al2O3 ceramics under fluorine plasma. J. Ceram. Soc. Jpn. 2009;117(1368):863-67.
- 4. Tan Y, Chen P, Zhu Z, Wu S, Tian Z. Plasma etching behavior of yttrium-aluminum oxide composite ceramics. International Journal of Applied Ceramic Technology. 2021;18(5):1710-15.
- 5. Qin X, Zhou G, Yang H, Wong JI, Zhang J, Luo D, et al. Fabrication and plasma resistance properties of transparent YAG ceramics. Ceram. Int. 2012;38(3):2529-35.
- 6. Miwa K, Sawai T, Aoyama M, Inoue F, Oikawa A, Imaoka K. Particle reduction using Y2O3 material in an etching tool. Paper presented at: 2007 International Symposium on Semiconductor Manufacturing; 15-17 October 2007; Santa Clara, CA, USA.
- 7. Kim Y-C, Kim C-I. Etching mechanism of Y2O3 thin films in high density Cl2/Ar plasma. J. Vac. Sci. Technol. A. Vacuum Surfaces Film. 2001;19(5):2676-79.
- 8. Miwa K, Takada N, Sasaki K. Fluorination mechanisms of Al2O3 and Y2O3 surfaces irradiated by high-density CF4/O2 and SF6/O2 plasmas. J. Vac. Sci. Technol. A. Vacuum Surfaces Film. 2009;27(4):831-35.
- 9. Kim D-M, Oh Y-S, Kim S, Kim H-T, Lim D-S, Lee S-M. The erosion behaviors of Y2O3 and YF3 coatings under fluorocarbon plasma. Thin Solid Films. 2011;519(20):6698-702.
- 10. Mitsuhiro Fujita KM. Plasma-resistant member for semiconductor manufacturing apparatus and method for manufacturing the same. U.S. Patent 6,838,405. 2005.
- 11. Kobayashi Y, Ichishima M, Yokoyama Y. Plasma resistant member. U.S. Patent 7,090,932. 2006.
- 12. Kim D-M, Lee S-H, Alexander WB, Kim K-B, Oh Y-S, Lee S-M. X-Ray Photoelectron Spectroscopy Study on the Interaction of Yttrium-Aluminum Oxide with Fluorine-Based Plasma. J. Am. Ceram. Soc. 2011;94(10):3455-59.
- 13. Kindelmann M, Weber ML, Stamminger M, Buschhaus R, Breuer U, Bram M, et al. Processing map to control the erosion of Y2O3 in fluorine based etching plasmas. J. Am. Ceram. Soc. 2022;105(5):3498-509.
- 14. Kindelmann M, Stamminger M, Schön N, Rasinski M, Eichel RA, Hausen F, et al. Erosion behavior of Y2O3 in fluorine-based etching plasmas: Orientation dependency and reaction layer formation. J. Am. Ceram. Soc. 2020;104(3):1465-74.
- 15. Cao Y-C, Zhao L, Luo J, Wang K, Zhang B-P, Yokota H, et al. Plasma etching behavior of Y2O3 ceramics: Comparative study with Al2O3. Appl. Surf. Sci. 2016;366(304-09.
- 16. Guillon O, Gonzalez-Julian J, Dargatz B, Kessel T, Schierning G, Räthel J, et al. Field-Assisted Sintering Technology/Spark Plasma Sintering: Mechanisms, Materials, and Technology Developments. Adv. Eng. Mater. 2014;16(7):830-49.
- 17. Bram M, Laptev AM, Mishra TP, Nur K, Kindelmann M, Ihrig M, et al. Application of Electric Current-Assisted Sintering Techniques for the Processing of Advanced Materials. Adv. Eng. Mater. 2020;22(6)
- 18. Liu Q, Liu J, Li J, Ivanov M, Medvedev A, Zeng Y, et al. Solid-state reactive sintering of YAG transparent ceramics for optical applications. J. Alloys Compd. 2014;616(81-88.
- 19. Li J-G, Ikegami T, Lee J-H, Mori T. Low-Temperature Fabrication of Transparent Yttrium Aluminum Garnet (YAG) Ceramics without Additives. J. Am. Ceram. Soc. 2004;83(4):961-63.
- 20. Stamminger M. Fluorocarbon plasma erosion of silica glass doped with aluminum, Bochum: Ruhr University Bochum; 2020.
- 21. Kindelmann M, Weber ML, Stamminger M, Buschhaus R, Wessel E, Bram M, et al. The role of fluorination during the physicochemical erosion of yttria in fluorine-based etching plasmas. J. Eur. Ceram. Soc. 2022;42(2):561-66.

- 22. Cockayne B. The uses and enigmas of the Al2O3-Y2O3 phase system. Journal of the Less Common Metals. 1985;114(1):199-206.
- 23. Kindelmann M. Field assisted sintering of yttria ceramics for plasma etching applications, Jülich: Forschungszentrum Jülich GmbH; 2021.
- 24. Storms HA, Brown KF, Stein JD. Evaluation of a cesium positive ion source for secondary ion mass spectrometry. Anal. Chem. 1977;49(13):2023-30.
- 25. Mogab CJ, Adams AC, Flamm DL. Plasma etching of Si and SiO2—The effect of oxygen additions to CF4 plasmas. J. Appl. Phys. 1978;49(7):3796-803.
- 26. Fearn S. An Introduction to Time-of-Flight Secondary Ion Mass Spectrometry (ToF-SIMS) and its Application to Materials Science, San Rafael, CA: Morgan & Claypool Publishers; 2015.
- 27. Williams DB, Carter CB. Transmission Electron Microscopy, New York: Springer; 2009.